Title	Physical experimental static testing and structural design optimisation for a composite wind turbine blade
Author(s)	Fagan, Edward M.; Flanagan, M.; Leen, Sean B.; Flanagan, Tomas; Doyle, Adrian; Goggins, Jamie
Publication Date	2016-12-10
Publication Information	Fagan, E. M., Flanagan, M., Leen, S. B., Flanagan, T., Doyle, A., & Goggins, J. (2017). Physical experimental static testing and structural design optimisation for a composite wind turbine blade. Composite Structures, 164, 90-103. doi: https://doi.org/10.1016/j.compstruct.2016.12.037
Publisher	Elsevier
Link to publisher's version	https://doi.org/10.1016/j.compstruct.2016.12.037
Item record	http://hdl.handle.net/10379/15609
DOI	http://dx.doi.org/10.1016/j.compstruct.2016.12.037

Physical Experimental Static Testing and Structural Design Optimisation for a Composite Wind Turbine Blade

E. M. Fagan [a,c,d], M. Flanagan [a,c,d,e], S. B. Leen [b,c,d], T. Flanagan [e], A. Doyle [e], J. Goggins [a,c,d]

[a] Civil Engineering, National University of Ireland Galway, Ireland.
[b] Mechanical Engineering, National University of Ireland Galway, Ireland.
[c] Centre for Marine and Renewable Energy Ireland (MaREI), Galway, Ireland.
[d] Ryan Institute for Environmental, Marine and Energy Research, Galway, Ireland.
[e] ÉireComposites Teo., Údarás Industrial Estate An Choill Rua, Inverin, Galway, Ireland.

* Corresponding author: Tel: +353 91492609, Email: Jamie.Goggins@nuigalway.ie

Abstract

This study presents experimental testing on a 13 m long glass-fibre epoxy composite wind turbine blade. The results of the test were used to calibrate finite element models. A design optimisation study was then performed using a genetic algorithm. The goal of the optimisation was to minimise the material used in blade construction and, thereby, reduce the manufacturing costs. The thickness distribution of the composite materials and the internal structural layout of the blade were considered for optimisation. Constraints were placed on the objective based on the stiffness of the blade and the blade surface stresses. A variable penalty function was used with limits derived from the blade test and the structural layout of the turbine. The model shows good correspondence to the test results (blade mass within 6% and deflection within 9%) and the differences between test and model are discussed in detail. The genetic algorithm resulted in five optimal blade designs, showing a reduction in mass up to 24%. Structural modelling in combination with numerical search algorithms provide a powerful tool for designers and demonstrates that the reader can have confidence in the claimed potential savings when the reference blade models are calibrated against physical test data.

Keywords: optimisation, genetic algorithm, FRP composites, Puck criterion, structural testing, wind turbine

1 Introduction

Even as the scale of wind turbine blades is reaching for and exceeding the 60 m, mark there is considerable demand for medium-sized turbines. A recent review [1] of the current wind energy sector placed emphasis on the advantages of smaller scale wind turbines. The authors claim that smaller scale turbines are suitable for meeting domestic and commercial energy needs in a grid system that has less local environmental impact than large scale wind farms. The blade under investigation in this study is 13 m in length for a 225 kW rated turbine, placing the turbine in the medium commercial range of device size. One of the major disadvantages for smaller wind turbines is the high initial and maintenance costs, a major component of which is the blades. A combination of structural testing and finite element (FE) modelling can be used to help reduce these costs through improvements to the blade design.

Full-scale structural testing is used in the blade certification process to help ensure a reliable and secure blade design. The IEC 61400-23 [2] international standard for testing provides an outline of the structural design requirements that blades must meet. A primary requirement for the blades, and the one that is the focus of the present study, is the structural response under static loading. A number of

authors have presented results from such static blade testing. Overgaard et al [3] performed a static test to collapse of a 34 m wind turbine blade in order to investigate the ultimate failure modes. Yang et al [4] performed similar testing to failure for a 40 m wind turbine blade and found that a complex series of failure modes resulted from an initial debonding of the adhesive joints of the outer aerodynamic shells. Larwood and Musial [5] report on static and fatigue structural testing of 12 m blades, identifying several regions of the blades for failures quite early in the fatigue tests. The blades are the key component in the turbines and failures in the blade structure are among the most common failure types during operation [6]. Failures in the blades can lead to significant downtime for the turbine and, due to the often remote location of wind turbines, it may not be a simple operation to repair a damaged blade, or worse, replace one completely [7].

In addition to full-scale structural testing, computational modelling methods have the potential to improve on standard blade designs. The most common form of modelling wind turbine blades uses 3D plane stress shell elements to represent the thin-walled composite laminates from which the blade is comprised. The plane stress assumption is quite valid for wind turbine blades, except for complex regions with significant through-thickness stresses such as the root-hub connection of the blade. Many authors have taken this approach and used it to develop parametric blade models for investigating various structural and aerodynamic aspects of the design. Bonnet and Dutton [8] demonstrated the adaptability of the combination of the Python scripting language and Abaqus finite element software in the generation of parametric blade models. Montesano et al [9] developed a methodology incorporating micromechanical material modelling and continuum damage mechanics and showed how parameters such as chord length and twist angle of the blade can affect the damage distribution. Vucina et al [10] have developed a methodology for the custom shape design of wind turbine blades to achieve maximum energy production. This approach to modelling has been shown to be robust, demonstrating good correspondence between tests and models [11] [12], and can investigate various aspects of blade structural and aerodynamic design.

The modelling methods presented in this study have been developed from a tidal turbine blade design methodology [13], [14]. The methodology generates parametric FE models of blades from basic design information, such as chord length, twist angle and aerodynamic load distributions. In order to assess the risk of failure, the FE models include a check for fibre failure and inter-fibre matrix failure based on the Puck failure criterion. The criterion is a ply-level (meso-scale) analysis and consists of five multi-axial stress interaction equations which define failure surfaces for the different failure modes [15]. The criterion defines three modes of failure for matrix cracking, depending on the combination of transverse and shear stress in the ply. Some failure modes, such as matrix cracking, are often tolerable in a structure. However, the failure mechanisms can induce local deterioration in the laminates which can act as the starting point for more serious failures, e.g. matrix cracking leading to local delaminations [16]. The failure analysis is performed by the user-defined subroutine UVARM in the commercial FE program Abaqus for each elemental integration point.

In this paper, a genetic search algorithm is used for the structural optimisation task to take advantage of the parametric models, and the large design space they represent. Genetic algorithms effectively provide a directed random search through a complex design space [17]. The directed aspect is due to the user-defined objective function which is a measure of preference of one design over another. The effectiveness of this optimisation method for complex composite laminates has been demonstrated over the last two decades. For example, it has been applied to problems of variable thickness distribution in composite structures [18] and combinatorial problems with multiple materials and varying fibre direction [19]. Some authors have focused specifically on wind turbine blades for structural and aerodynamic design. Pourrajabian et al [20] focused closely on the aerodynamic effects

of varying blade designs, using beam theory for structural analysis to reduce computational effort. Barnes and Morozov [21] investigated novel internal structural layouts for wind turbine blades in an effort to reduce mass. Fischer et al [22] describe their tool for a multi-objective optimisation of the annual energy production, blade mass and rotor thrust. These all demonstrate how optimisation tools can be combined with aerodynamic, structural or power performance tools to study complex blade design problems.

The goal of the present study is to apply a genetic search algorithm, aided with an advanced failure analysis, to the problem of wind turbine blade structural design. The parametric blade models that enable the design optimisation are first compared to the results from a static structural test of a 13 m blade. The details of the test campaign are provided and the differences between model and test results are investigated. The design features explored in the optimisation relate to the internal blade structure and the thickness of the laminates used in the blade construction. The objective of the design study is to reduce the mass of the wind turbine blade without degradation of the structural performance.

2 Methodology

The design methodology is outlined in four parts:

(i) A description of the details of the wind turbine blade geometry.
(ii) An overview of the design loads and the mechanical test loads.
(iii) Details on the construction of the parametric FE models.
(iv) An explanation of the genetic algorithm and the details of its operation.

2.1 Blade definition

The wind turbine blade examined in this study is based on the Vestas V27 turbine with a standard power rating of 225 kW. The blade was manufactured using a novel “one-shot” manufacturing process [23]. Commonly, the manufacture of wind turbine blades involves producing several distinct parts, which are then assembled together to form the blade. The one-shot approach involves polymerising the entire structure, including the embedded metal inserts at the root, in one single process, thereby eliminating the need for gluing. Further details on the advantages and disadvantages of the one-shot process for the manufacture of large scale composite structures are available in the review by Flanagan et al [23].

The blades are constructed from glass-fibre (GF) with a powder epoxy resin. Steel inserts in the root of the blade provide a connection to the turbine hub. The blades follow the normal structural convention for wind turbines with a box spar providing flexural and torsional stiffness and with the aerodynamic outer shells forming the blade shape. The box spar is made up of the spar caps, with unidirectional (UD) plies oriented along the length of the blade, and webs which provide shear strength to the structure. The shear webs are constructed from triaxial layers of GF-epoxy; each triaxial layer consists of the layup $[0°/\pm 45°]$ oriented to the length of the blade. In the FE analysis, each triaxial layer is made up of three plies of UD, with the appropriate orientations applied. The outer shell is composed of layers of the triaxial weave with an imbedded balsa core towards the tip. Figure 1 shows the various regions in detail on a cross-section of the blade.

Table 1 reports the in-plane stiffness values for a unidirectional layer of the GF-epoxy material. Table 1 also indicates the material properties for the balsa wood core layer and the gelcoat. The balsa wood increases the panel buckling resistance in the aerodynamic shell laminates and the gelcoat is used for

protecting the outer surface of the blade from environmental damage [24]. Table 2 shows the composite layups for the three main sections of the blade, i.e. the spar caps region, the outer aerodynamic shells and the shear webs. The number of unidirectional and triaxial plies at each radial blade station are noted as well as the locations of the core material. The layups used in the optimisation study take a more generic form and are detailed in full in Section 2.4.1.

A study by Sandia National Labs [25] on the costs associated with wind turbine blades indicated that, for large wind turbine blades (30 m in length and greater), the combined costs of materials and labour contributed approximately 68% to the total costs of each blade. The materials costs cover such items as the unidirectional and double-bias glass-fibre mat materials, gelcoat for surface protection, balsa core material, resin and the root attachment system. The labour costs were estimated based on the work flow, labour hours and equipment requirements for manufacturing each of the separate blade components, assembling the blade, finishing, inspection, shipping and testing of the blade. The remaining 28% of the total overall blade costs were associated with design development, manufacturing plant overhead and blade transportation. This figure for costs of materials and labour has been confirmed to be accurate with respect to the blade under investigation in the present study and was used to determine the total percentage saving per blade achieved by the optimisation methodology.

Table 3 outlines the geometry of the blade and includes the radial distributions of the chord length, twist angle, aerodynamic profiles and blade thickness. The centreline of the spar caps is located at approximately 32% of the chord length along the entire length of the blade. All of the necessary details to model the blade were determined either from the masters theses of Mohamed [26] and Froyd [27] or correspondence with the industrial partner.

2.2 Test and load definition

Structural testing of wind turbine blades involves applying an equivalent mechanical load to match the aerodynamic loading the blade experiences during operation. In typical static testing, the loads are applied via weights, cranes, hydraulic or electronic actuators connected to the blade at a number of load points [28]. The greater the number of load points, the more accurately the bending moment distribution is reproduced. Figure 2 shows the set-up for the static test performed on the 13 m wind turbine blade. In this set-up, two blades are mounted on a support structure and are loaded using chains and chain blocks. The load is transferred to each blade through three load saddles. The load saddles contain plywood inserts which match the aerodynamic profile of the blade at the load application points. Silicone sheeting was placed between the blade surface and the plywood inserts in order to ensure an even distribution of load across the blade surface and to avoid any stress concentrations due to the clamping force. One major advantage for the chosen set-up is the lower cost, achieved by reacting one blade off of the other and, hence, significantly reducing the reactive loads on the support structure. One caveat to the testing is that the support structure was not bolted to the floor and the weight of the blades was supported by trolleys positioned at 10 m along each blade. Some error was introduced into the blade deflection measurements due to movement of the reaction frame; however, this was recorded and corrected for in the presented results.

The load saddles were located at 5 m, 10 m and 12 m from the root of the blade. The IEC test standard [2] states that one of the key areas of interest in the blade is the region inboard up to where the change in cross-section slows down. On the blade under investigation this includes the blade from root up to approximately 9 m. Since the load saddles typically invalidate the results of the blade tests locally (due to induced stress concentrations not experienced in operation) the outer two load saddles were

located at 10 m and 12 m. The chain block attached to each load saddle was adjusted to match the target load sequentially. When all three load saddles reached their respective targets, the deflections were recorded. Since the two blades were mounted with the same orientation, they experienced different loading. The first blade was loaded with a positive bending moment and the second with a negative bending moment referring to the flapwise direction (see Figure 2). Only the results for the blade with positive flapwise bending moment, the left hand blade in Figure 2, are presented since this configuration is representative of the blade loading during operation. The blades were monitored for any signs of failure during the test, such as cracking, surface buckling or acoustic emissions. No such signs of failure were observed and the blades passed the test for certification.

Normal operation of the turbine is for wind speeds between 3.5 and 25 m/s, with a nominal wind speed of 14 m/s, after which the turbine uses a pitch control system to maintain constant power production. The test loading on the blade was determined from a report by Riso contained in [26] and is shown in Figure 3 (a). The test loads were determined from an expression for the wind load on the blade for an extreme 50 m/s gust. Figure 3 (a) also shows the magnitude of the forces applied to the blade at the load saddle locations. Figure 3 (b) shows a comparison of the bending moment profiles along the blade for both load types. The bending moment on the blade due to the load saddles is slightly higher (up to 13.4 kNm at 2 m along the blade) than that due to the original wind loads indicating that the testing is conservative in nature. In the design optimisation study, the original wind loading is applied to the models, not the test loading. The three test loads (acting on a much smaller area) may induce local non-linear behaviour, hence the wind loads are more representative of the actual operational loads of the turbine.

The aerodynamic lift and drag forces experienced by a wind turbine blade can be resolved into the forces in the flapwise (perpendicular to the rotor plane) and lead(-lag)wise (parallel to the rotor plane) directions [29]. The lead(-lag)wise forces contribute to the torque driving the turbine, while the flapwise forces comprise the thrust acting on the blade. The thrust is the most significant force acting on the blade. The static test is restricted to testing the blade in the flapwise direction only. Hence, further testing to account for the lead(-lag)wise loading (and high-cycle fatigue testing for lifetime assessment) is necessary to fully analyse the response of the structure under all loading conditions. Table 4 shows the distribution of the wind loads along the length of the blade.

2.3 FE Model Set-up

The blades are made up of 3D lofted shell sections. The composite layups are then applied to the shells in the FE models. This enables the development of parametric models for the quick and efficient evaluation of a design's structural response. Computational efficiency is a key driver of the methodology due to the large number of models required for the optimisation study. The FE models are generated using a Python code developed in-house. The inputs to the code include:

- Chord length distribution along the blade,
- Aerodynamic twist distribution along the blade,
- Location of the leading edge of the blade in the x- and y-directions,
- Distribution of airfoils along the blade, and the chord-normalised coordinates for each airfoil designation,
- Distribution of the location and width of the spar caps (normalised by the chord length),
- Distribution of the number and location of the shear webs,
- Material properties and layup sequences for each radial blade section,
- Flapwise and lead(-lag)wise loads on the blade,
- Mesh and FE job analysis settings.

The code automatically generates the full FE model and performs the analysis. Any of these parameters can easily be considered for optimisation. However, the study presented here focuses on the thickness distribution of the laminates and number of shear webs. Due to the large number of potential layup sequences, this is an expansive design space for the search. Post-processing of the results is also conducted using Python. The code has been previously used in the analysis of small-scale wind turbine blades [30] and concept tidal turbine blades [14] and is well suited for parametric studies.

The loads are applied to the blade using a form of multi-point constraint (MPC). All of the nodes in the section where the load is applied are constrained to a single reference point onto which the force is applied as a point load. The coupling distributes the load between the reference point and the nodes in the section. The root of the blade is constrained in all six degrees of freedom.

The blade models use a combination of 4-node reduced integration (S4R) plane stress linear shell elements with hourglass control and 3-node triangular (S3) linear shell elements. A mesh convergence study was conducted as part of the development of the FE models, using the blade tip deflection as the convergence criterion. From the study it was determined that a mesh with approximately 19500 elements (18800 nodes) was suitable for accurately modelling the test set-up. This level of mesh refinement utilised elements with a side length of approximately 40 mm.

2.4 Genetic Algorithm Optimisation

The genetic algorithm (GA) is used to evaluate a population of randomly generated potential designs. Then, applying genetic operations, it searches through the design space to find the optimum solution to the problem. The flowchart in Figure 4 outlines the steps in the GA:

- Generate the initial population of potential designs.
- Evaluate the relative potential fitness of each individual in the population and rank the population.
- Evolve the population for the next generation by the following methods:
    - Retain the best individuals.
    - Cross pairs of individuals to create new individuals.
    - Randomly mutate the design variables of some of the population.
- Evaluate the relative potential fitness of the new population and repeat the previous step until the stop criterion is reached.
- Further analyse the optimum blade design.

The following sections provide a detailed description of the key processes involved in the genetic search algorithm under the headings: *genetic encoding, crossover, gene mutation, elitist selection* and *objective function*.

2.4.1 Genetic encoding

Each potential blade design is completely defined by a design vector which consists of thirty-two variables. These variables define the distribution of biaxial and triaxial layers in the blade. Biaxial layers are formed from two unidirectional plies with a layup oriented $\pm 45°$. In the optimised blades, biaxial layers replace the triaxial layers used in the shear webs of the original blade. Since the webs predominantly support the blade in shear, the biaxial layers provided a similar level of support while using less material.

The thirty-two variables in the design vector are split into four categories. The first three categories relate to the outer shells, the spar caps and the shear webs respectively and each are made up of ten design variables. The last category contains two variables that relate to the blade as a whole. Table 5

defines each of the variables and indicates each variable's upper and lower limit. The categories for the variables are defined as follows:

1. The first ten design variables define the number of triaxial layers in the outer shells.
2. The next ten variables define the number of unidirectional plies in the spar caps.
3. The next ten variables define the number of biaxial layers in the shear webs.
4. The second last variable defines the end point of the balsa core in the shear webs and the last variable defines the number of shear webs in the blade.

All of the variables are integer values within the set limits. The description alongside each variable in Table 5 indicates what type of composite layer it relates to and to what region it is applied.

The schematic in Figure 5 outlines the convention used in setting up the blade's composite structure. The three levels to the hierarchy are defined as *S* for the radial section along the blade, *R* for the region within a blade section (e.g. suction side leading edge laminate) and *L* for layer in each region (where the layers are numbered from the outer aerodynamic surface inwards). Defining ten design variables for each structural component means there are ten possible locations for ply drop-offs (discrete locations where the thickness of the composite laminates change). The radial sections are located evenly along the length of the blade; these locations range from 2 m to 12 m along the blade in 1 m intervals.

In order to maintain ply continuity along the blade, the design variables define the number of plies for a certain length of the blade. For example, Figure 5 demonstrates a general case of the spar cap laminates. The variable x_{11} refers to the number of unidirectional layers that span the entire length of the blade (from S_0 to S_{10}). The variable x_{12} refers to the number of layers spanning the blade from S_0 to S_9 and so on until the final variable, x_{20}, defines the number of unidirectional plies in the region spanning from S_0 to S_1.

2.4.2 Crossover

In order to create the next generation's population, a crossover method is applied. The method used in this work is known as fitness proportionate selection or roulette wheel selection. An individual's probability of being chosen as parent is based on its fitness value; the better the fitness, the higher the chance it will be used to create a new individual. With this method there is still a chance that a less fit individual may be selected as a parent, which may prove beneficial overall if the weak solution has some component that is favourable to the new child. New individuals are generated from two parent individuals. The crossover involves setting a split point at a random location in the parents' vectors of design variables. Then the child inherits all of the design variables to the left of the crossover point from the male parent and all of the design variables to the right of the crossover point from the female parent.

2.4.3 Gene mutation

Once the new population has been generated, each variable in each individual in the population has a small chance of a random mutation. The mutation, if it occurs, is constrained by the original limits on the design variables (Table 5). The objective of the mutation is to further promote genetic diversity and to explore the design space around any local optima. This can also help to avoid early convergence and has the largest impact on the results in later generations.

For each design variable in an individual, a random number is generated between zero and one. If the number is smaller than the chance of mutation (m), then the variable's value is reassigned. For this

study, the value of m is varied based on the number of generations evaluated. The following equation describes the variation in m over the course of the analysis:

$$m(g) = m_i + (m_f - m_i)^{\frac{g_f}{g}} \quad (2)$$

where $m(g)$ is the chance of mutation at the current generation, m_i is the chance of mutation at the beginning of the analysis, m_f is the chance of mutation at the end of the analysis, g_f is the total number of generations and g is the current generation. Figure 6 shows the results of the power law function as it increases from the initial value for the chance of mutation to the final value over the course of the analysis. With this function the change in the chance of mutation only becomes significant after the analysis has proceeded through approximately 60% of the generations. The higher chance of mutation is considered beneficial in the latter stages of the analysis in order to avoid premature convergence and to promote localised searching about the optimum solutions determined so far.

2.4.4 Elitist selection

Several varieties of elitist selection are used in practise, e.g. single, multiple and variable elitist strategies. A single elitist method works by retaining the fittest parent in the new generation in place of the weakest new individual. In multiple elitist methods, a number of parents may be retained. On the other hand, in variable elitist strategies, the retention rate varies during the analysis, e.g. as a function of the number of generations. Soremekun et al [31] studied the effectiveness of several such strategies and found the multiple elitist method to perform the strongest. This method performed well in terms of number of optima found for a particular problem, effectiveness at searching through a large number of similar near-optimum designs and in terms of overall computational effort. This multiple elitist method involves retaining the top designs from the parent population and placing them into the new population and simply generating the number of child designs to refill the population to its original number. This is less computationally expensive than other methods where a whole new child population is generated and ranked and then the best parent designs replace the weakest child designs. In this study, five individuals from the previous generation with the highest fitness were retained into the new population.

2.4.5 Objective function

The objective function is used to evaluate the performance of each individual. Providing an appropriate evaluation function for the optimisation problem is the task of the designer and requires a strong understanding of the problem at hand. The goal of this study is to minimise the mass of the blade, and, hence, reduce the manufacturing costs.

If the design space is the complex landscape formed by the limits of the design variables, then the solution space is the resulting landscape after the evaluation of the results of each of those potential designs. The solution space can be considered to be made up of three regions: the feasible space, the infeasible space and the illegal space. Illegal solutions do not meet the design constraints and can't be considered as viable designs, e.g. a blade that fails one or more material failure criteria. Infeasible solutions have met the basic criteria for a solution, but are still outside of the limits set by the design, e.g. a blade with a large tip deflection which could negatively impact the turbine aerodynamics. Often the optimum solution lies on the border between the infeasible and feasible regions. In order to keep some infeasible solutions in the population a penalty is applied to the objective function values of individuals that exceed the tip deflection from the physical test. The objective function is given by:

$$\min\left(f(\boldsymbol{x}) = M(\boldsymbol{x})p(\boldsymbol{x}) \right) \tag{2}$$

where $M(\boldsymbol{x})$ is the mass of the blade, $\boldsymbol{x}$ is the vector of design variables for each individual and $p(\boldsymbol{x})$ is the penalty function given by,

$$p(\boldsymbol{x}) = e^{\frac{\delta_{tip} - \delta_{test}}{\delta_{test}}} \quad for\ p(\boldsymbol{x}) \geq 1 \qquad p(\boldsymbol{x}) = 1 \quad for\ p(\boldsymbol{x}) < 1 \tag{3}$$

where δ_{tip} is the tip deflection of the current individual and δ_{test} is the tip deflection of the blade from the static test. The penalty function is only applied when it exceeds a value of one. The function exponentially increases with increasing tip deflection. However, an additional legality constraint is placed on the tip deflection to account for the limited allowable distance to avoid tip fouling (the blade tip striking the tower). This limit is 2.5 $\delta_{tip,test} \approx 1.5m$. These inherent limits on the deflection act as a means of quantifying the distance metric for the constraint. The distance metric is described by Smith and Coit [32] as a means of determining the closeness of a solution to feasibility. Other penalty methods exist which apply a linear penalisation or take a power law approach to the problem (such as those outlined by Herath et al [33]), but the exponential function method worked well for this study.

A legality constraint is applied to the stresses in the blade laminates. The values of the risk of failure (stress exposures) for FF and IFF are calculated for the outer plies of the blade and factors of safety are applied. If the risk values exceed the set limits then that individual is deemed illegal and is removed from the population before the evolution stage.

The failure criterion defined by Puck [15] is phenomenologically based. The criterion provides a robust and effective approach to the prediction of failure in composites based on extensive testing of composites and using the brittle fracture theory of Mohr as its basis. It is made up of five stress interaction equations, two to determine the risk of fibre failure (FF) in tension and compression and three to determine the risk of different forms of inter-fibre failure (IFF) occurring [15]. The equations defining the risk of failure (or stress exposure) for FF are:

$$f_E(FF)^+ = \frac{1}{\varepsilon_{1T}}\left(\varepsilon_1 + \frac{\nu_{12}}{E_1} m_{\sigma f}\sigma_2\right) \tag{4}$$

$$f_E(FF)^- = \frac{1}{\varepsilon_{1C}}\left|\left(\varepsilon_1 + \frac{\nu_{12}}{E_1} m_{\sigma f}\sigma_2\right)\right| + (10\gamma_{12})^2 \tag{5}$$

where $f_E(FF)^+$ and $f_E(FF)^-$ refer to the stress exposure values for tension and compression respectively; ε_{1T} and ε_{1C} refer to the failure strain in tension and compression, respectively; ε_1 is the in-plane longitudinal strain; σ_2 is the in-plane transverse stress; γ_{12} is the in-plane lamina oriented engineering shear strain ($(10\gamma_{12})^2$ is an empirical correction factor); ν_{12} is the major Poisson's ratio; E_1 is the in-plane fibre direction modulus and $m_{\sigma f}$ is the mean stress magnification factor.

IFF can be separated into three distinct types: Mode A, Mode B and Mode C, which depend on the combined state of transverse and shear stress in the laminate. Mode A IFF refers to a tensile transverse stress and shear stress combination, Mode B a combination of compressive transverse

stress and shear stress and Mode C is a similar compressive-shearing stress state though with significantly higher compressive stress, generally resulting in failure of the laminate. The three equations for IFF are:

$$f_E(IFF)_A = \sqrt{\left(\frac{\tau_{12}}{S_{12}}\right)^2 + \left(1 - p^{(+)}_{\parallel\perp}\frac{Y_T}{S_{12}}\right)^2\left(\frac{\sigma_2}{Y_T}\right)^2} + p^{(+)}_{\parallel\perp}\frac{\sigma_2}{S_{12}} \quad (6)$$

$$f_E(IFF)_B = \frac{1}{S_{12}}\left(\sqrt{\tau_{12}^2 + \left(p^{(+)}_{\perp\parallel}\sigma_2\right)^2} + p^{(-)}_{\perp\parallel}\sigma_2\right) \quad (7)$$

$$f_E(IFF)_C = \left[\left(\frac{\tau_{12}}{2\left(1 + p^{(-)}_{\perp\perp}\right)S_{12}}\right)^2 + \left(\frac{\sigma_2}{Y_C}\right)^2\right]\frac{Y_C}{(-\sigma_2)} \quad (8)$$

where $f_E(IFF)_A$, $f_E(IFF)_B$ and $f_E(IFF)_C$ refer to the stress exposure values for the three modes of IFF; σ_2 and τ_{12} refer to the in-plane transverse and shear stress in the laminate, respectively; S_{12} is the in-plane shear strength of the ply; Y_T is the transverse tensile strength; Y_C is the transverse compressive strength; and $p^{(+)}_{\parallel\perp}$, $p^{(+)}_{\perp\parallel}$, $p^{(-)}_{\perp\parallel}$ and $p^{(-)}_{\perp\perp}$ are parameters for controlling the shape of the failure envelope formed by the three equations [34]. The values of the all of the material parameters necessary for assessing glass-fibre epoxy laminates are contained in Table 6. The Puck failure criterion has been shown to be effective when paired with an optimisation procedure [35]. When used to identify first ply failure (FPF) in a buckling study of composite plates it produced optimum designs satisfying both FPF strength and buckling requirements over other material failure criteria.

A factor of safety of two was applied to both of the FF stress exposure values. Similarly, for the three inter-fibre failure modes, if the value in any of the blade's laminates exceeds 0.75, then the legality constraint is violated. The failure criterion are calculated in the FE program using UVARM, a user-defined subroutine for generating output variables. Any of the regular output quantities for the integration point (such as stress, strain, displacement, etc.) are available to UVARM. The UVARM code produces six output variables: the five stress exposure values and a marker variable to indicate the mode of IFF the element is within range of.

2.4.6 Genetic algorithm operating parameters

Table 7 contains general information on the search performed. The total number of individuals in the population was set at 25. The total number of generations for each optimisation problem was 300, while the number of retained individuals in the multiple elitist scheme for each generation was 5 and the chance of mutation varied from 0.03 to 0.05 according to Equation 2. The GA was implemented in Python to easily interface with the parametric FE model generation code and Abaqus.

3 Results and Discussion

3.1 Model Validation

Figure 7 shows the results of the static test on the 13 m wind turbine blade along with the associated FE model results. The blade deflections are shown for the maximum load applied. A comparison of the results at the load saddle locations indicates that the FE model overestimated the blade deflections by 9% (56 mm) at the 12 m load saddle. This implies that the physical blade is stiffer than the FE model predicts. During the test, the blade rotated relative to the support structure, which was only

noted once the test was completed. It is believed that the deflection results may be overestimated by up to 24 mm at the outer load saddle location, due to this error. The load deflection curve for the three load saddles is shown in Figure 8. The three curves are linear in nature and in combination with manual inspection of the blades during testing indicate that no damage or non-linear deflection occurred for the extreme load. The kinks in the curves for the 5 m and 10 m saddles are due to the issue with fixing the rotation of the root connection fixture.

The mass of the physical blade and blade model was compared as part of the model validation. The mass of the blade components modelled (excluding the metal inserts) is approximately 529 kg, while the numerical model's mass is 497 kg, a difference of 6%. The discrepancies between the blade model and the physical blade may be attributed to several factors:

- Additional glass-fibre material added during the manufacturing procedure, but not accounted for in the original manufacturing documents.
- A slight variability in material density and fibre volume content, which is inherent in the production of composite structures.
- Additional non-structural material which was omitted from the FE models.
- The through-thickness stresses in the root region are not accounted for by plane stress elements.

The results from the blade model are used as the reference for comparison with the design optimisation results in the following sections.

3.2 Optimisation Results

3.2.1 Optimum blade designs from GA

Table 8 shows the optimised values of the design variables after application of the GA. Five near-optimum solutions (objective function values within approximately 0.5%) were found using the multiple elitist method described in Section 2.4.4. The final generation contained a number of additional designs with high levels of competitiveness. The variables x_1 to x_{10}, controlling the thickness of the outer shells, show no variation between the five optimum designs. Since the outer shells don't significantly contribute to the overall stiffness of the blade, it is not surprising that these variables have nearly all reached the minimum possible value. There is more variation in variables x_{11} to x_{20}, which control the thickness of the spar caps. However, the differences in these variables are minimal, with only x_{13}, x_{14} and x_{19} varying slightly. The variables controlling the shear web thicknesses, x_{21} to x_{30}, are also all quite similar and, since they are all close to their lower limits, indicate that they do not significantly affect the fitness of their blade designs. Variable x_{31} controls the location of the drop-off of the balsa layer in the shear web and was found to be close to a minimum in all but the second solution. The last variable x_{32} indicates that all five blade designs have only one shear web. This is a promising result as manufacturing a blade with only a single web using the one-shot process is less complex and costly than with two webs.

Table 9 shows the layups for spar caps, outer shells and shear web for the Solution 1 blade. The number of unidirectional, triaxial and biaxial plies are indicated for each radial section as well as the gelcoat and core layers. The table demonstrates how the encoding of the thirty-two design variables is used to generate the blade layups. Table 10 shows the results for the five optimum blade designs. The results include: the fitness value, blade mass, tip deflection, tip rotation, the maximum values of each of the five stress exposures, the radial location of the blade centre of mass and the generation when each design was first found. The results for fitness, mass and tip deflection were as follows:

- Solution 1 resulted in the best fitness value (387.2 kg). The design demonstrated a mass saving of 22.9% (113.9 kg) from the reference blade. However, this resulted in a tip deflection of approximately 809 mm, and was subsequently penalised.
- The next fittest design showed a saving in mass from the reference blade of 22.8% (113.3 kg). This blade design also resulted in a tip deflection of approximately 809 mm.
- Solution 3 resulted in a mass saving of 24.1% (120 kg) and a tip deflection of 824 mm.
- Solution 4 resulted in a mass saving of 24.1% (119.8 kg) and a tip deflection of 823 mm.
- Solution 5 resulted in a mass saving of 22.3% (111 kg) and a tip deflection of 807 mm.

The cost saving per blade is also shown in Table 10. The optimisation resulted in savings of between 15.1% and 16.3% of the total costs of the blade, due to the reduction in material required and the associated labour costs.

All of the designs were found to be slightly on the infeasible side of the solution space. A more severe penalisation method would drive the GA to finding only solutions that meet this constraint; however, the current penalty method was applied since some leeway is allowed in the final deflection of the blade. Several of the alternative designs in the final population demonstrated a feasible tip deflection of 800 mm or less. However, the best fitness value among these solutions was 412.6 kg, with a mass saving of 17% from the reference blade design. This indicates the strong influence the penalty function has in controlling the results of the genetic search and the added flexibility granted by approaching the optimum from the infeasible space, as well as the feasible.

The tip rotation was determined to be approximately 10.6°, with the five optimum designs showing little variation between them (~0.1°). The tip rotation of the reference blade was approximately 7.9° in magnitude. The difference between the optimum and reference blades is attributed to the optimum designs all containing only a single shear web and the reduced thickness of their outer shells. Both of these factors reduce the torsional stiffness of the optimum blade designs. Since the loading situation under investigation is an extreme gust, and not an operational wind speed, the degree of twist is not a major concern. Further investigation of the response of the structure should be conducted to determine the level of twist in the blade for operating wind loads, since added twist could significantly affect the aerodynamics of the turbine. Table 10 also shows the radial location of the centre of mass of the blade designs. Large changes in the location of the centre of mass may affect the dynamics of the turbine. The largest change in radial location from the reference blade was 160 mm towards the tip, resulting from solutions 3 and 4.

The results for the five stress exposure values for each of the blades showed little variation, indicating the stresses in the blades to be of similar magnitude. The stress exposure values for FF in tension and compression were the lowest of all the failure modes, with the value of the stress exposure for compressive failures slightly higher than for tensile. A factor of safety was applied to the stress exposures for the three IFF modes, which limited their values to 0.75. The result was that the GA found designs bordering on this upper limit for Mode A IFF. The five designs show values between 0.720 and 0.743. The stress exposure values for Mode B and C are lower, with values of 0.234 and 0.238, respectively. Modes A and B of IFF are generally considered a tolerable failure mode. However, the current design was specified to avoid all possible failures for the extreme load case. The optimum blade designs showed a decrease in the stress exposure values from the reference blade for the FF failure modes and Mode B IFF.

From Table 10 it can be seen that many of the designs are close to the optimum, but with slightly varying design variables. As noted by Soremekun [31], for the blade bending problem, the outermost plies have the greatest effect on the design's fitness value and adding inner plies may not significantly

change the results. Therefore, it's possible to end up with many solutions with high fitness values, but slightly varying composite layups. The higher chance of mutation in the last number of generations is intended to locally explore the design space around the optimum solutions. Table 10 shows the generation that each of the optimum blade designs was first determined. Solutions 3 and 4 were determined first, at generation 175 and 176, respectively. By retaining these individuals into the following generations, and using them in the crossover process, their strong structural characteristics were further exploited. Solutions 1, 2 and 3 were then determined at generation 190, 195 and 192, respectively.

A number of the blade designs in the final population which met the overall design criterion also showed the onset of local buckling in the shear web towards the root of the blade. A similar situation was reported by Barnes and Morozov [21], who outlined a number of options for including bucking checks, including: incorporating a buckling constraint using design formulae, conducting an additional eigenvalue analysis or including additional high modulus material options in the design variables. Future work will extend the GA to include a buckling load factor or a constraint on the ratio of length to thickness of the shear web panels to avoid buckling.

Figure 9 shows a comparison between the thickness of the spar cap laminates for the reference and the optimum blade (Solution 1) designs. Figure 10 shows the thickness variations of the laminates in the optimum blade; the same layups are applied to both the suction and pressure sides of the blades. The GA resulted in relatively evenly spaced drops in the thickness of the UD material over the length of the blade. Stress concentrations appear in locations with a large drop in thickness. The largest single drop in thickness occurs at 11 m on the optimum blade.

3.2.2 Blade Analysis

The following results are displayed for Solution 1. Figure 11 shows the distribution of the fibre direction stress (σ_{11}) along the centreline of the spar caps for the optimum blade and reference blade designs. As can be seen from Figure 9, the thickness of the two blade designs is not significantly different up to 9 m on both blades. The result is a similar stress distribution in both blades up to this location. The stress is nearly symmetric for the pressure and suction sides of the blade and is below 45 MPa for the majority of the blade. The reduction in thickness of the laminates towards the tip of the blade has a notable effect on the stresses with a major spike at the 11 m location in the optimum blade. The root region of the optimum blade also shows higher stresses than the reference blade; however, the stresses are of a similar magnitude to the rest of the spar caps. The drop in thickness of the spar caps near the root in the reference blade also causes a large spike in stress, which is not evident in the optimum blade design.

Figure 12 shows contour plots of the distribution of the fibre direction strain (ε_{11}) in the plies on the outer surface of the optimum blade at the maximum load applied. The strain is highest along the spar caps and does not exceed 0.23% in tension or compression over the blade. Stress concentrations can be seen where the cross-sectional shape of the blade changes from circular to the aerofoil shape at the root. The geometry in this region is complex and may not be fully captured by the parametric models. Future work will investigate mesh smoothing options to obtain a closer approximation to the geometry of the blade in this location.

Figure 13 shows a contour plot of the stress exposure values for Mode A inter-fibre failure. The risk of IFF Mode A is higher on the suction side of the blade (the side in compression) than the pressure side. Most notably, the trailing edge laminates along the length of the blade experience both transverse and longitudinal compression and may be under risk of local buckling. At approximately 3

m along the blade, there is a stress concentration where the spar cap meets the outer shell. This region requires closer inspection to avoid possible delamination between shells and spar cap during operation.

3.2.3 GA performance

Figure 14 shows the progression of the fitness of the population during optimisation. The shaded area indicates the upper and lower bounds of the objective function values for the population at each generation. The fitness of the population improves rapidly in the first 25 generations and by generation 50 the GA has already determined several designs with improvements in fitness from the reference blade. The large range of the fitness values in the last generations is caused by the higher chance of mutation. As seen in the previous section, the multiple elitist scheme is capable of finding multiple optima per analysis run. Future work will investigate the precision/accuracy trade-off for the GA and determine the most effective values for the genetic operators. This will help determine the total number of generations required by the algorithm to determine optimum solutions and minimise computational time. Although the genetic operators are often problem specific, the study by Soremekun et al [31], which examined the trade-off between computational cost and search effectiveness, was useful in initially determining the GA parameters.

At several points in the analysis illegal individuals were generated through either crossover or mutation processes. Examination of the illegal individuals indicated Mode A IFF failures for many of the designs. As noted in the results in Table 10, the highest stress exposure values were for IFF Mode A with the GA converging on results bordering the design limit value of 0.75. Therefore, it is not surprising that individuals with higher values of $f_E(IFF)^A$ were generated. Several blade designs were also found with tip deflections beyond the limit of 2.5 δ_{test}, which would lead to tip fouling.

The total number of models analysed in the GA search was approximately 3300. Since a number of designs were retained each generation, significant computational savings were made by not re-running previously completed analyses. This led to a saving of approximately 34% of the total possible computational time. All computations were performed on an Intel core i7 desktop computer with 8 CPUs and 16 GB RAM. Each single analysis took approximately 1 minute to generate the model, run the analysis and post-process the results and the entire search took approximately 55 hours to complete.

4 Conclusion

The present study demonstrates the effectiveness of pairing a genetic search algorithm (GA) with parametric finite element models for composite wind turbine blades. The FE models were successfully calibrated against test data, working with the manufacturers to ensure the models accurately reflect the structural makeup of the blade. The models and test showed good correspondence for the mass and deflection data and the differences between blade model and physical blade were discussed in detail. The static structural testing showed the current blade design is sufficiently durable for an extreme 50 m/s gust loading. The most significant findings from the design optimisation include:

- The GA determined a number of potential design options and resulted in a mass saving of 23% for the optimum blade design.
- The optimum blade resulted in a saving of approximately 15.5% on the total blade manufacturing costs due to the reduction in mass of glass-fibre epoxy required.

- Due to the application of constraints on the optimisation this improvement in mass subsequently results in a slight increase in blade deflection and in blade surface stresses.
- The multiple elitist scheme preserved a number of good designs (five) through each generation, resulting in the GA finding several near-optimum designs for further analysis.
- It was found that a single shear web was sufficient in all five of the optimum designs. From a manufacturing perspective this represents an opportunity for reductions in complexity and cost.
- A combination of a relatively high number of retained designs and a variable chance of mutation of the design variables resulted in a good balance between global searching of the design space and localised searching around the optimum designs. This produced individuals with superior fitness values, especially in later generations when the chance of mutation was highest.
- The use of the Puck failure criterion enabled an analysis of the risk of failure of the plies in the blades for several different failure modes, providing additional constraints for the GA. The optimised blade models are within safety factors for fibre failure and inter-fibre failure (matrix cracking) of the laminates.
- A number of the designs in the final population exhibited the onset of local buckling in their shear web laminates, future work will include buckling checks as an additional constraint.
- Significant computational savings were made by storing the results from analyses for future reference.

The GA analysis will also be expanded to include additional load cases, such as combined flapwise and lead(-lag)wise loading and operational static and dynamic loading. The methodology has been proved effective for medium scale wind turbine blades and is equally applicable to other composite blades and propellers. Hence, future uses include the analysis and design of small/domestic scale (15 kW) wind turbine blades and large scale (1 MW) tidal turbine blades.

Acknowledgements

This material is in part based upon works supported by the Science Foundation Ireland Centre for Marine and Renewable Energy Ireland (MaREI) under Grant No. 12/RC/2302. It was also funded by a fellowship from the College of Engineering and Informatics, NUI Galway, and was supported by an NUI Travelling Studentship, 2014. The last author would like to acknowledge the support of Science Foundation Ireland through the Career Development Award programme (Grand No. 13/CDA/2200).

References

[1] Tummala A, Velamati RK, Sinha DK, Indraja V, Krishna VH. A review on small scale wind turbines. Renewable and Sustainable Energy Reviews 2016 ;56: 1351–71.

[2] International Electrotechnical Commision. Technical specification IEC TS 61400-23 wind generator systems - part 23: full-scale structural testing of rotor blades. 2001.

[3] Overgaard LCT, Lund E, Thomsen OT. Structural collapse of a wind turbine blade. Part A: Static test and equivalent single layered models. Composites Part A: Applied Science and Manufacturing 2010 ;41: 257–70.

[4] Yang J, Peng C, Xiao J, Zeng J, Xing S, Jin J, et al. Structural investigation of composite wind turbine blade considering structural collapse in full-scale static tests. Composite Structures 2013 ;97: 15–29.

[5] Larwood SM, Musial W. Comprehensive Testing of Nedwind l2-meter Wind Turbine Blades at NREL. 19th American Society of Mechanical Engineers (ASME) Wind Energy Symposium 2000: 297–305.

626 [6] Ciang CC, Lee J-RJ, Bang HH-J. Structural health monitoring for a wind turbine system: a
627 review of damage detection methods. Measurement Science and Technology 2008 ;19:
628 122001.

629 [7] Lu B, Li Y, Wu X, Yang Z. A review of recent advances in wind turbine condition monitoring
630 and fault diagnosis. Electronics and Machines in Wind 2009: 1–7.

631 [8] Bonnet P, Dutton G. Parametric Modelling Of Large Wind Turbine Blades. Proc. 21st Abaqus
632 UK Reg. User Meet., Daventry, UK: 2007, p. 211–25.

633 [9] Montesano J, Chu H, Singh CV. Development of a physics-based multi-scale progressive
634 damage model for assessing the durability of wind turbine blades. Composite Structures
635 2016;141: 50–62.

636 [10] Vucina D, Marinic-Kragic I, Milas Z. Numerical models for robust shape optimization of wind
637 turbine blades. Renewable Energy 2016;87: 849–62.

638 [11] Jensen FM, Falzon BG, Ankersen J, Stang H. Structural testing and numerical simulation of a
639 34m composite wind turbine blade. Composite Structures 2006;76: 52–61.

640 [12] Overgaard LCT, Lund E. Structural collapse of a wind turbine blade. Part B: Progressive
641 interlaminar failure models. Composites Part A: Applied Science and Manufacturing 2010 ;41:
642 271–83.

643 [13] Fagan EM, Kennedy CR, Leen SB, Goggins J. Damage mechanics based design methodology
644 for tidal current turbine composite blades. Renewable Energy 2016 ;97: 358–72.

645 [14] Fagan EM, Leen SB, Kennedy CR, Goggins J. Finite element based damage assessment of
646 composite tidal turbine blades. J. Phys. Conf. Ser., vol. 628, 2015, p. 12106.

647 [15] Puck A. Failure Analysis of FRP Laminates by means of Physically based Phenomenological
648 Models. Composites Science and Technology 1998 ;58: 1045–67.

649 [16] Renard J, Thionnet A. Damage in composites: From physical mechanisms to modelling.
650 Composites Science and Technology 2006 ;66: 642–6.

651 [17] Gen M, Cheng R. Genetic Algorithms and Engineering Optimization. vol. 7. 2000.

652 [18] Paluch B, Grédiac M, Faye A. Combining a finite element programme and a genetic algorithm
653 to optimize composite structures with variable thickness. Composite Structures 2008 ;83: 284–
654 94.

655 [19] Lund E, Stegmann J. On structural optimization of composite shell structures using a discrete
656 constitutive parametrization. Wind Energy 2005 ;8: 109–24.

657 [20] Pourrajabian A, Nazmi Afshar PA, Ahmadizadeh M, Wood D. Aero-structural design and
658 optimization of a small wind turbine blade. Renewable Energy 2015 ;87: 837–48.

659 [21] Barnes RH, Morozov EV. Structural optimisation of composite wind turbine blade structures
660 with variations of internal geometry configuration. Composite Structures 2016 ;152: 158–67.

661 [22] Fischer GR, Kipouros T, Savill AM. Multi-objective optimisation of horizontal axis wind
662 turbine structure and energy production using aerofoil and blade properties as design variables.
663 Renewable Energy 2014 ;62: 506–15.

664 [23] Flanagan MH, Doyle F, Fagan E, Goggins J, Leen SB, Doyle A, et al. Large Scale Structural
665 Testing of Wind Turbine Blades Manufactured Using a One- Shot Out-Of-Autoclave Process.
666 Proc. Civ. Eng. Res. Irel. Conf., Galway, Ireland: 2016.

[24] Bir GS, Lawson MJ, Li Y. Structural design of a horizontal-axis tidal current turbine composite blade. ASME 30th International Conference on Ocean, Offshore, and Arctic Engineering 2011: 14.

[25] TPI Composites. Cost Study for Large Wind Turbine Blades : WindPACT Blade System Design Studies SAND2003-1428 2003.

[26] Mohamed AA. Modelling of Vestas V27-225kW wind turbine blade. MSc Thesis, University of Stavanger, Stavanger, Norway, 2011.

[27] Frøyd L. Control System on a Wind Turbine. MSc Thesis, Norwegian University of Science and Technology, Trondheim, Norway, 2009.

[28] Zhou HF, Dou HY, Qin LZ, Chen Y, Ni YQ, Ko JM. A review of full-scale structural testing of wind turbine blades. Renewable and Sustainable Energy Reviews 2014 ;33: 177–87.

[29] Rooij R Van. Terminology, Reference Systems and Conventions. Report to: European Commission Contract JOR3-CT98-0284. TU Delft: 2001.

[30] Fagan EM, Leen SB, Torre O De La, Goggins J. Experimental investigation and numerical modelling of domestic scale wind turbine blades. Proc. Civ. Eng. Res. Irel. Conf., Galway, Ireland: n.d.

[31] Soremekun G, Gürdal Z, Haftka RT, Watson LT. Composite laminate design optimization by genetic algorithm with generalized elitist selection. Computers & Structures 2001 ;79: 131–43.

[32] Smith AE, Coit DW. Penalty functions. Handbook of Evolutionary Computation 1995 ;97: c5.

[33] Herath MT, Natarajan S, Prusty BG, John N St. Isogeometric analysis and Genetic Algorithm for shape-adaptive composite marine propellers. Computer Methods in Applied Mechanics and Engineering 2015 ;284: 835–60.

[34] Puck A, Kopp J, Knops M. Guidelines for the determination of the parameters in Puck's action plane strength criterion. Composites Science and Technology 2002 ;62: 371–8.

[35] Deveci HA, Aydin L, Secil Artem H. Buckling optimization of composite laminates using a hybrid algorithm under Puck failure criterion constraint. Journal of Reinforced Plastics and Composites 2016 ;35: 1233–47.

List of Figures

Figure 5. Overview of the naming/numbering convention for processing the results of the FE analysis. TE = trailing edge, LE = leading edge. Sections are labelled radially along the blade from root to tip, regions are labelled counter-clockwise from the leading edge of the blade for each section and layers are labelled from the top surface of the laminate down for each region.

Figure 6. Variation in the chance of mutation for the design variables over the course of the genetic search (generations are normalised).

Figure 7. Blade deflection results from the static test and numerical model.

Figure 8. Load versus deflection curve for the three load saddles measured in the physical test of the blade.

Figure 9. Comparison of the thickness distribution in the spar caps along the length of the blades between the reference blade and the optimum blade design found by the GA.

Figure 10. Thickness distribution of the laminates in the optimum blade.

Figure 11. Fibre direction stress (σ_{11}) distribution along the centreline of the spar caps of the optimum and reference blades.

Figure 12. Contour plot of the fibre direction strain (ε_{11}) distribution on the outer surface of the blade at the extreme wind load.

Figure 13. Contour plot of the stress exposure values for inter-fibre failure Mode A ($f_E(IFF)^A$) on the outer surface of the blade at the extreme wind load.

Figure 14. Results from the GA search. The bounds for the minimum and maximum values of the objective function for each individual in the population are shown.

List of Tables

*Table 1. Mechanical properties of the various materials used in the blade models. * Triaxial layers were assumed to consist of three layers of UD material. The density of a single triaxial layer is slightly lower than a UD layer. ** Values for the mechanical properties of the gelcoat and core/balsa layers were obtained from* [24].

Table 2. Details of the composite layups for the three main sections of the blade, the spar caps, outer aerodynamic shells and the shear webs.

Table 3. The distributions along the length of the blade of some of the key geometric (and structural) data, including: chord length, twist angle, blade thickness and aerodynamic profiles [26]. *Note: Some of the quantities have been normalised. *** The thickness distribution of the blade along its length is determined by the chord length and the designation of NACA profile applied at each section.*

Table 4. Radial distribution of the out of plane loads on the wind turbine blade applied in the optimisation study [26].

Table 5. Outline of the design variables and their limits.

Table 6. Parameters required for Puck failure criterion.

Table 7. Information on the set-up of the genetic algorithm.

Table 8. The optimum values for each of the design variables from the genetic search algorithm.

Table 9. Details of the composite layups for Solution 1 optimum blade for the three main sections of the blade: the spar caps, outer aerodynamic shells and the shear webs.

Table 10. Breakdown of the results of the optimum designs found by the genetic algorithm.

Figures

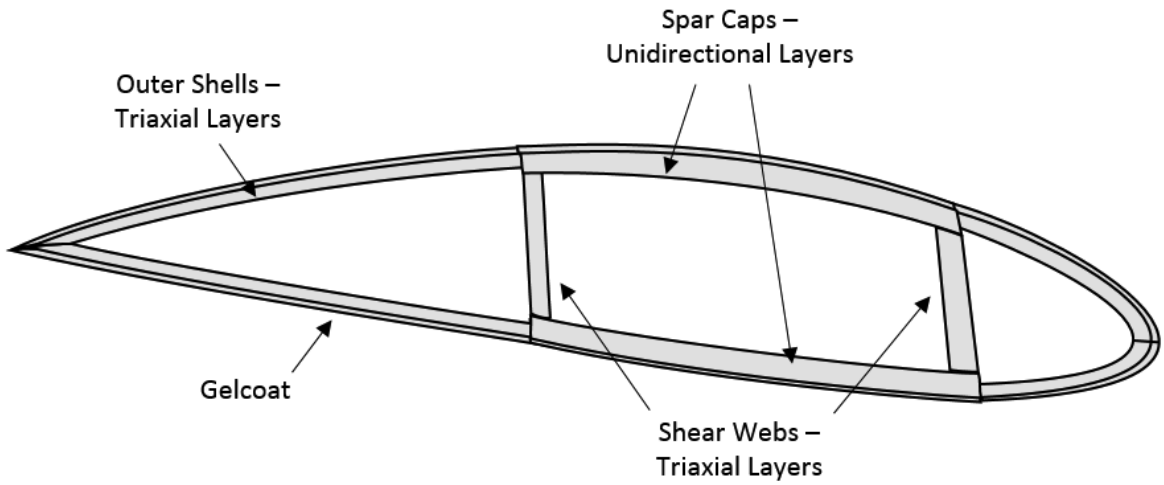

Figure 1. The principal layups for the three main sections of the wind turbine blade: the spar caps, shear webs and outer aerodynamic shells.

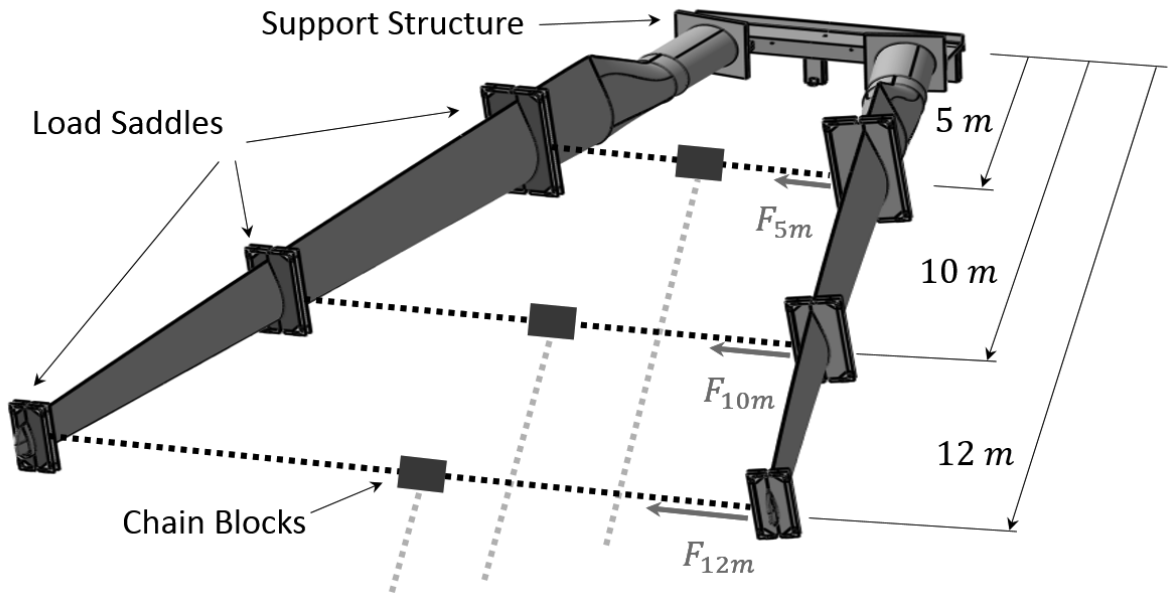

Figure 2. Set-up for the static test on the 13 m wind turbine blade.

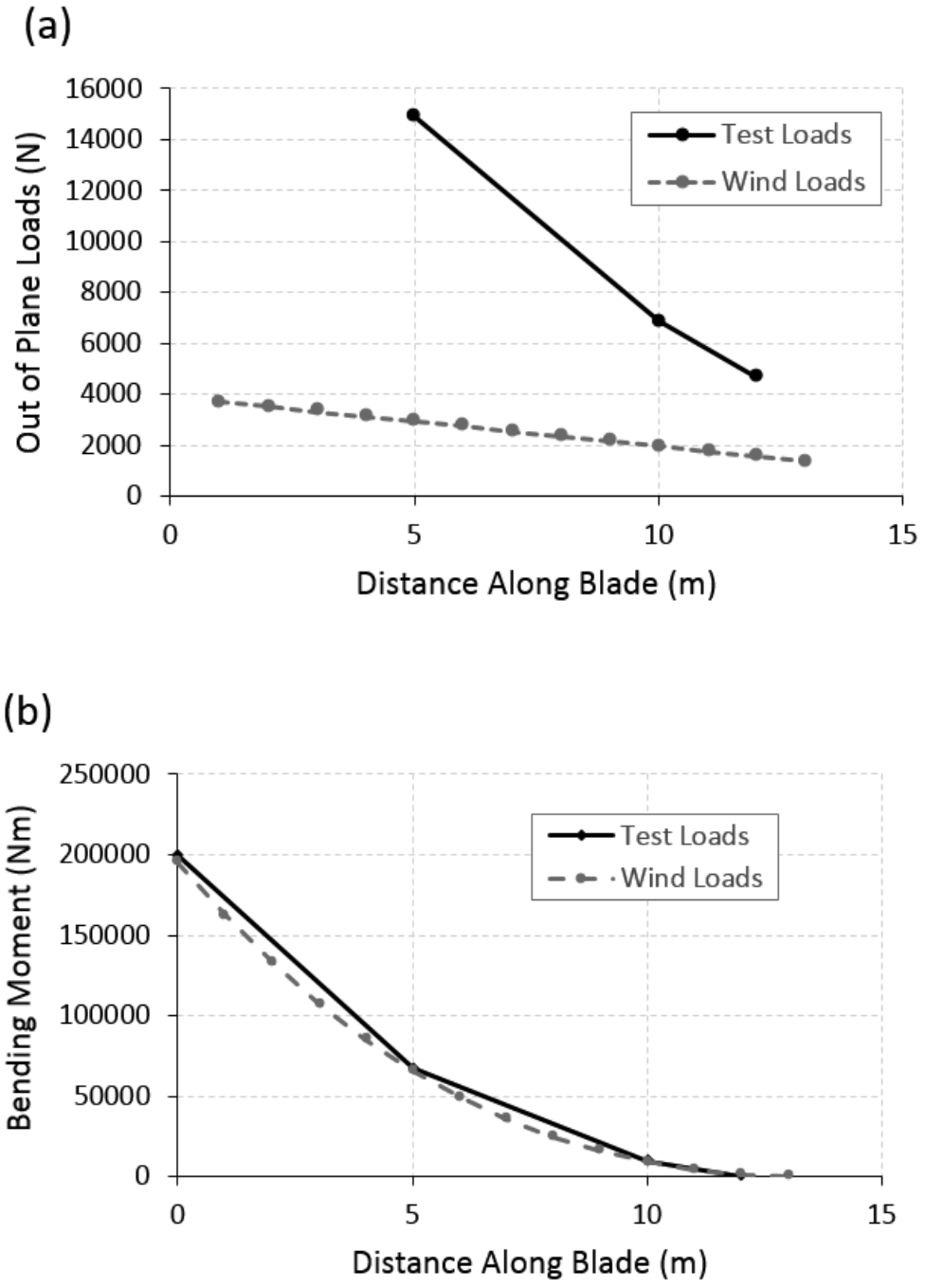

Figure 3. (a) Wind loads and mechanical test loads and (b) their respective bending moment profiles along the blade.

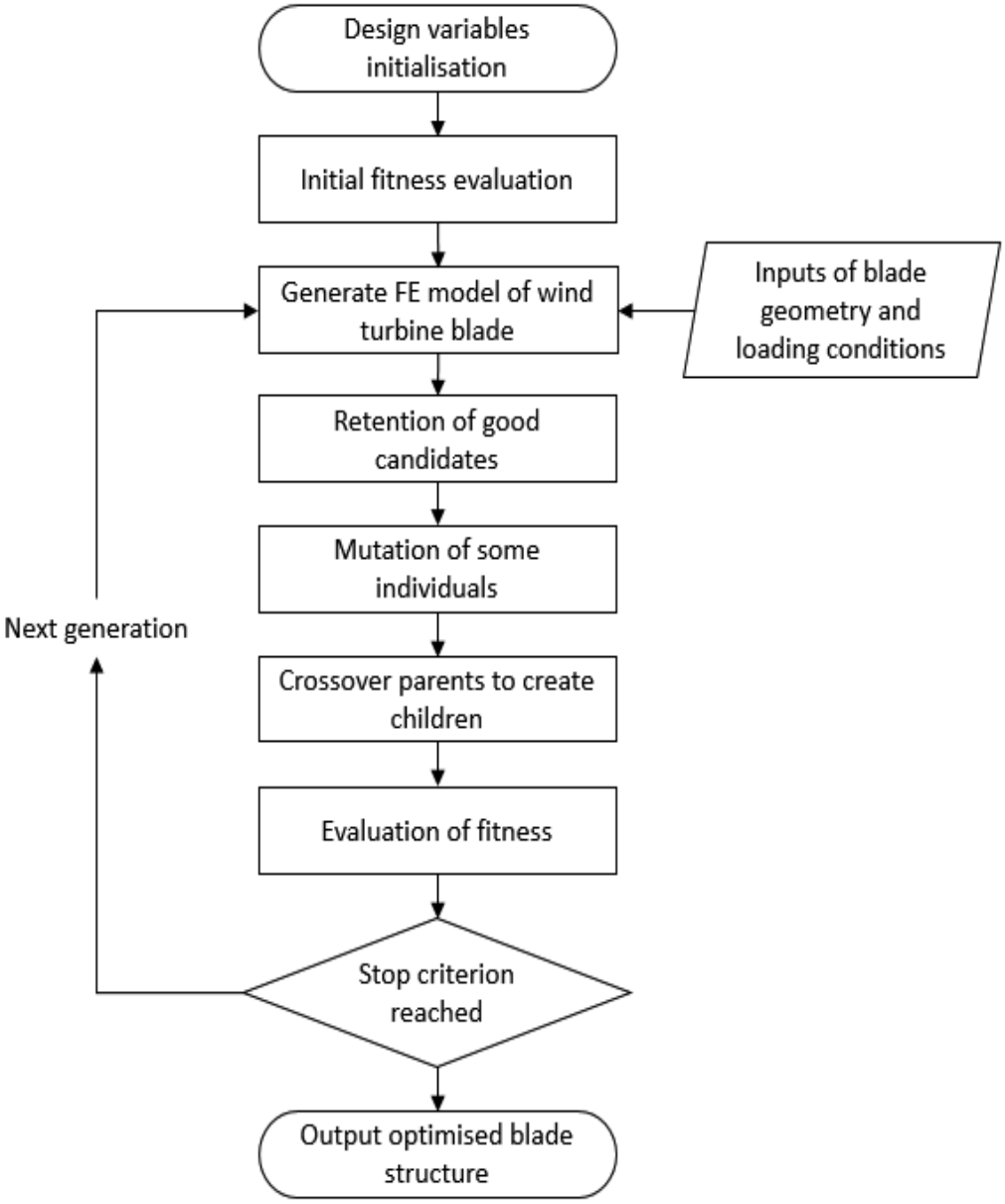

Figure 4. Flowchart describing the genetic algorithm's functions.

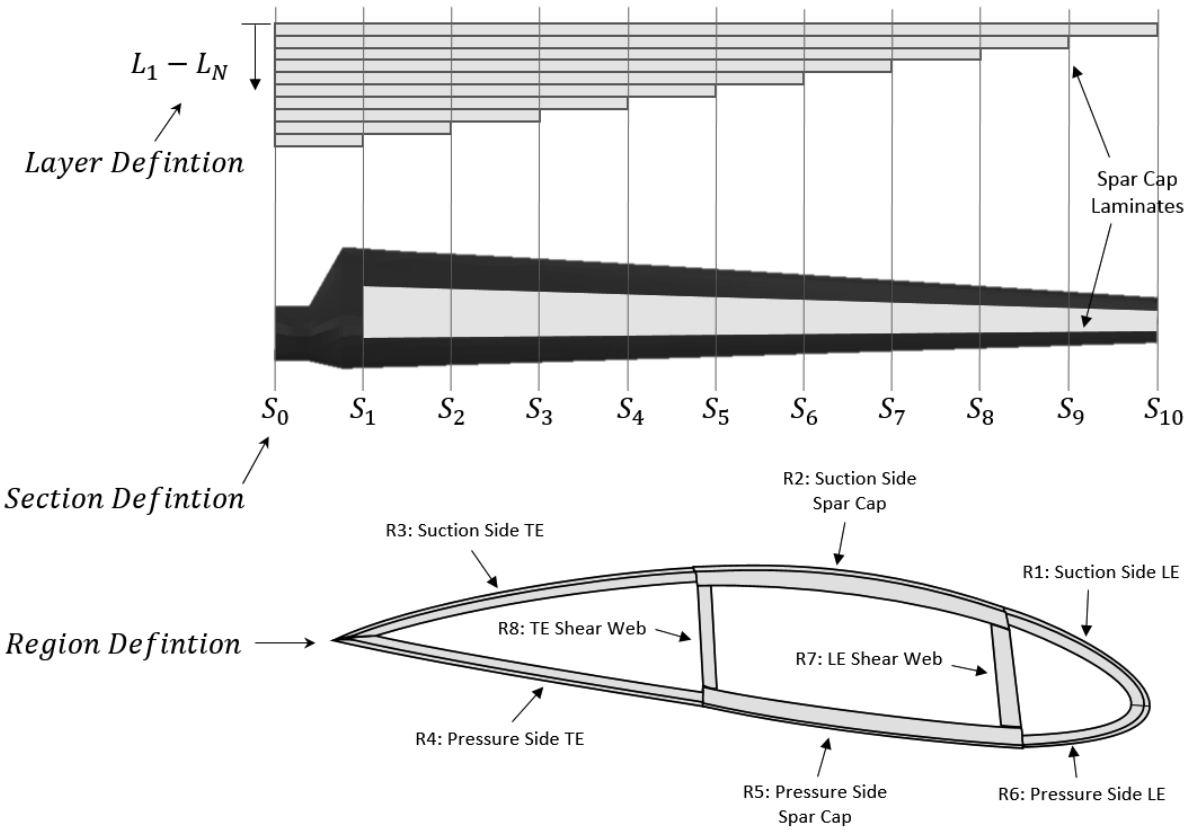

Figure 5. Overview of the naming/numbering convention for processing the results of the FE analysis. TE = trailing edge, LE = leading edge. Sections are labelled radially along the blade from root to tip, regions are labelled counter-clockwise from the leading edge of the blade for each section and layers are labelled from the top surface of the laminate down for each region.

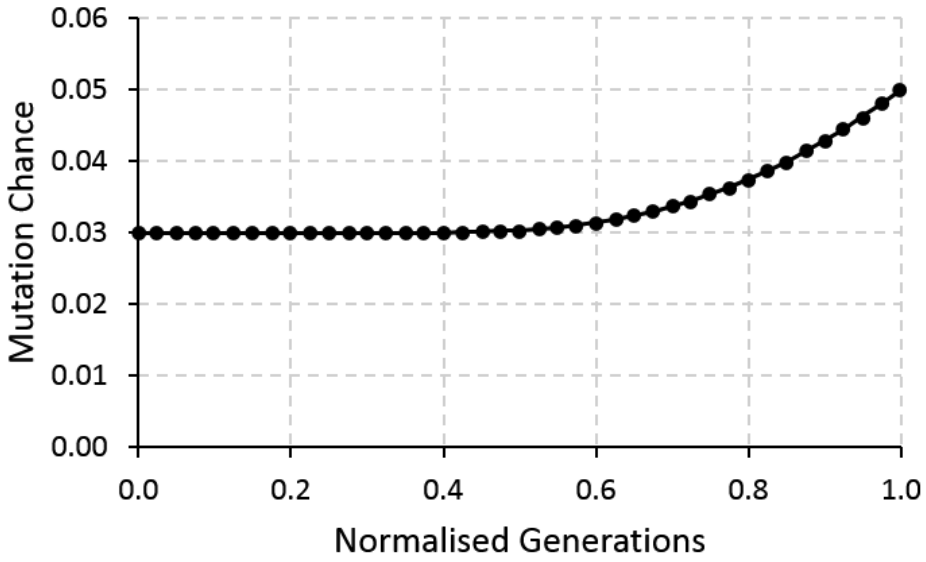

Figure 6. Variation in the chance of mutation for the design variables over the course of the genetic search (generations are normalised).

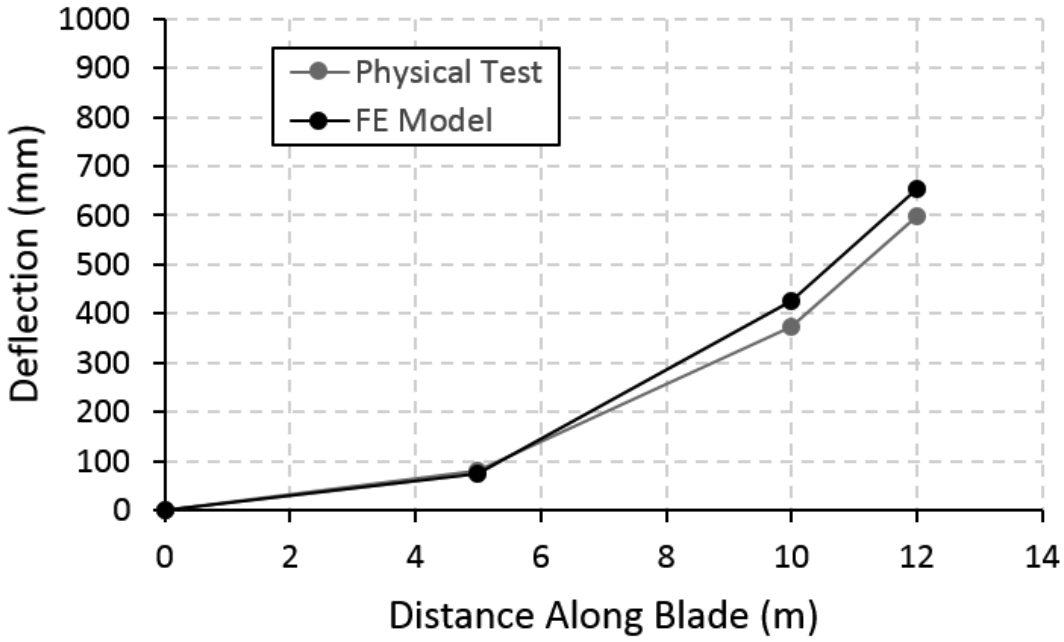

Figure 7. Blade deflection results from the static test and numerical model.

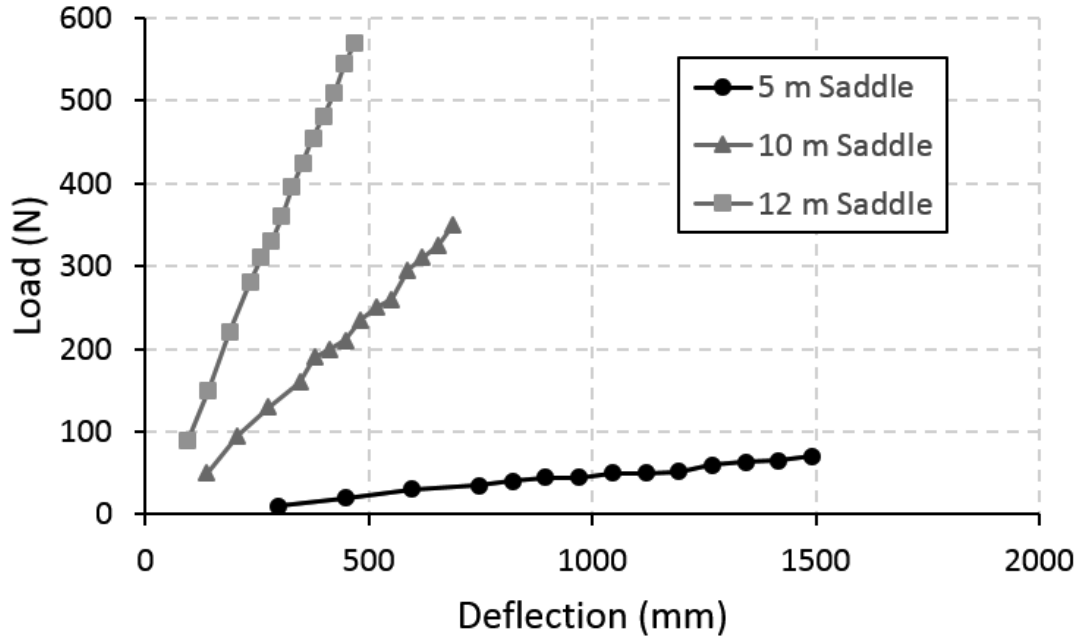

Figure 8. Load versus deflection curve for the three load saddles measured in the physical test of the blade.

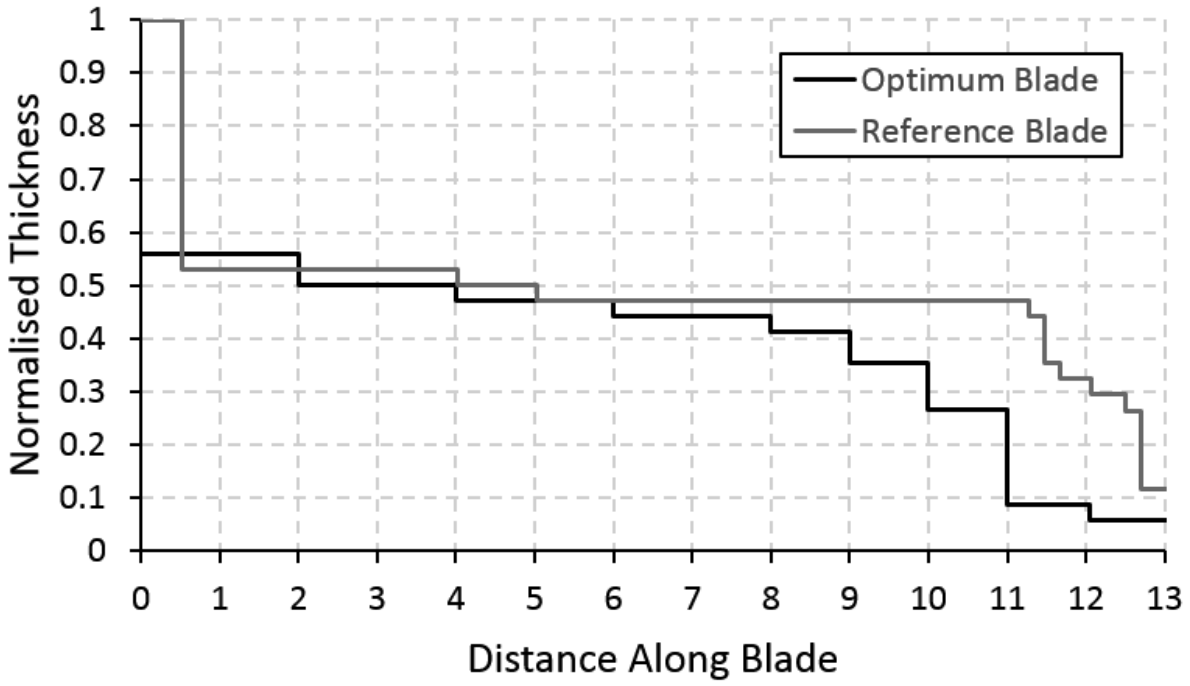

Figure 9. Comparison of the thickness distribution in the spar caps along the length of the blades between the reference blade and the optimum blade design found by the GA.

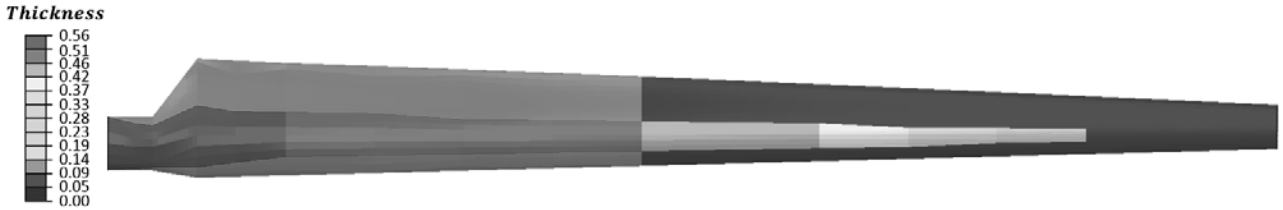

Figure 10. Thickness distribution of the laminates in the optimum blade.

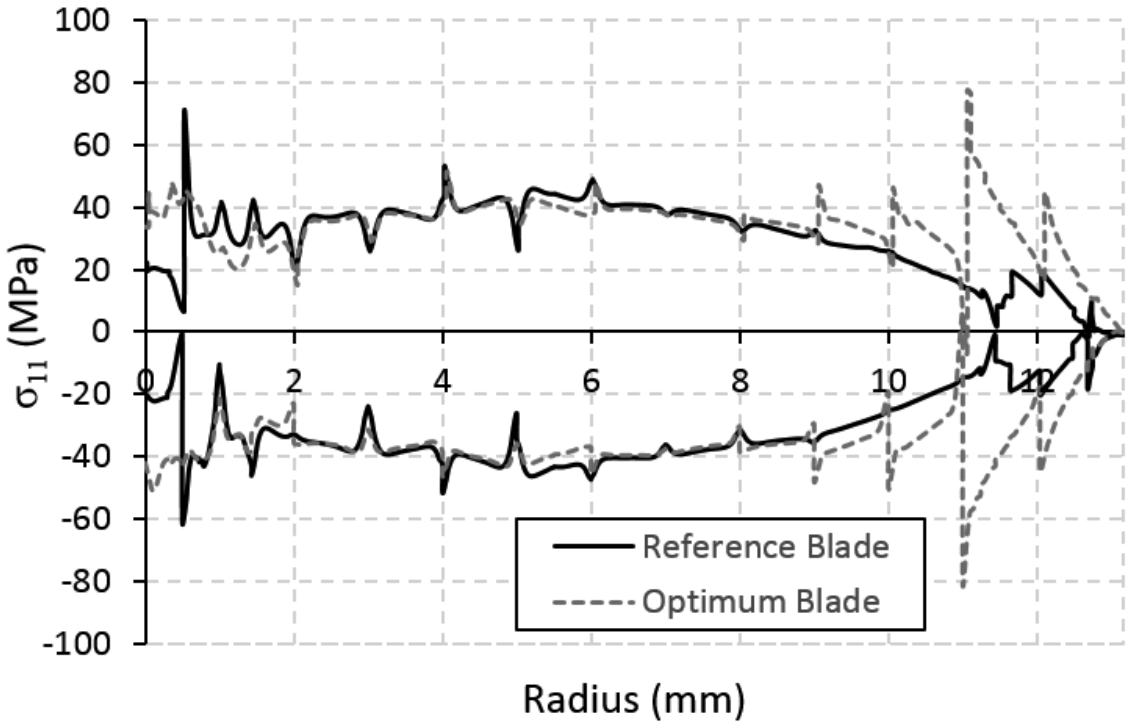

Figure 11. Fibre direction stress (σ_{11}) distribution along the centreline of the spar caps of the optimum and reference blades.

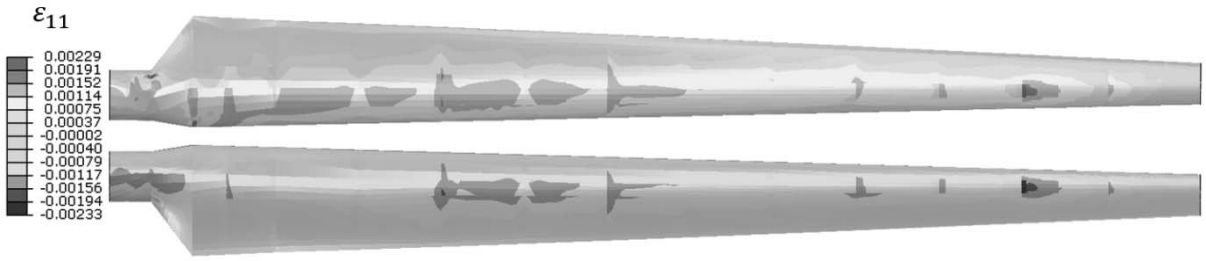

Figure 12. Contour plot of the fibre direction strain (ε_{11}) distribution on the outer surface of the blade at the extreme wind load.

Figure 13. Contour plot of the stress exposure values for inter-fibre failure Mode A ($f_E(IFF)^A$) on the outer surface of the blade at the extreme wind load.

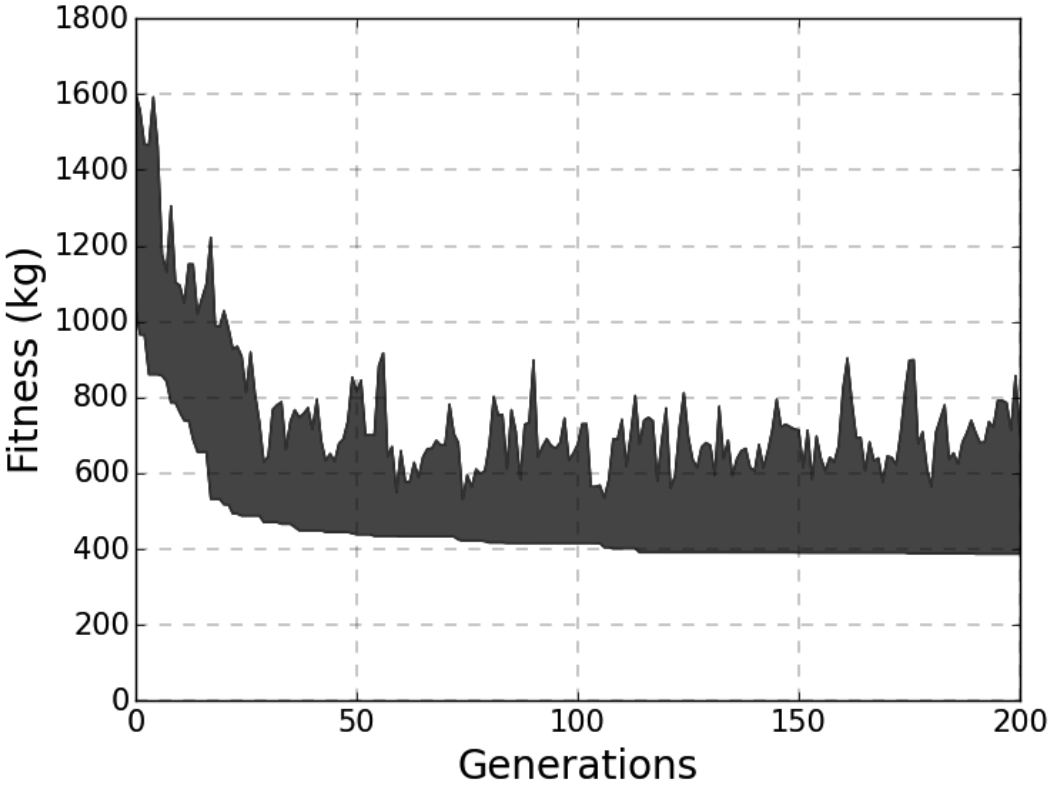

Figure 14. Results from the GA search. The bounds for the minimum and maximum values of the objective function for each individual in the population are shown.

Tables

*Table 1. Mechanical properties of the various materials used in the blade models. * Triaxial layers were assumed to consist of three layers of UD material. The density of a single triaxial layer is slightly lower than a UD layer. ** Values for the mechanical properties of the gelcoat and core/balsa layers were obtained from [24].*

	*UD **	*Gelcoat ***	*Balsa ***
E_1 *(MPa)*	35000	0.00001	10
E_2 *(MPa)*	11000	0.00001	10
G_{12} *(MPa)*	4000	0.000001	0.2
v_{12}	0.2	0.3	0.3
Density (kg/m³)	1900	1830	80

Table 2. Details of the composite layups for the three main sections of the blade: the spar caps, outer aerodynamic shells and the shear webs.

	Spar Caps					***Outer Shells***				***Webs***	
0.00	UD x 32	TRIAX x 2	Gelcoat								
1.00	UD x 16	TRIAX x 2	Gelcoat			TRIAX	Core	TRIAX	Gelcoat	UD x 4	TRIAX x 10
2.00	UD x 16	TRIAX x 2	Gelcoat			TRIAX	Core	TRIAX	Gelcoat	UD x 3	TRIAX x 10
3.00	UD x 16	TRIAX x 2	Gelcoat			TRIAX	Core	TRIAX	Gelcoat	UD x 2	TRIAX x 10
4.00	UD x 16	TRIAX x 2	Gelcoat			TRIAX	Core	TRIAX	Gelcoat	UD	TRIAX x 10
5.00	UD x 15	TRIAX x 2	Gelcoat			TRIAX	Core	TRIAX	Gelcoat	UD	TRIAX x 10
6.00	UD x 14	TRIAX x 2	Gelcoat			TRIAX	Core	TRIAX	Gelcoat	TRIAX x 4	
7.00	UD x 14	TRIAX x 2	Gelcoat			TRIAX	Core	TRIAX	Gelcoat	TRIAX x 4	
8.00	UD x 14	TRIAX x 2	Gelcoat			TRIAX	Core	TRIAX	Gelcoat	TRIAX x 4	
9.00	UD x 14	TRIAX x 2	Gelcoat			TRIAX	Core	TRIAX	Gelcoat	TRIAX x 4	
10.00	UD x 14	TRIAX x 2	Gelcoat			TRIAX	Core	TRIAX	Gelcoat	TRIAX x 4	
11.00	UD x 14	TRIAX x 2	Gelcoat			TRIAX	Core	TRIAX	Gelcoat	TRIAX x 4	
12.00	UD x 2	TRIAX x 2	Core	TRIAX x 2	Gelcoat	TRIAX	Core	TRIAX	Gelcoat	TRIAX x 4	
12.50	UD	TRIAX x 2	Core	TRIAX x 2	Gelcoat	TRIAX	Core	TRIAX	Gelcoat	TRIAX x 4	
13.00	TRIAX x 4	Gelcoat				TRIAX x 4	Gelcoat			TRIAX x 4	
13.15	TRIAX x 4	Gelcoat				TRIAX x 4	Gelcoat				

*Table 3. The distributions along the length of the blade of some of the key geometric (and structural) data, including: chord length, twist angle, blade thickness and aerodynamic profiles [26]. Note: Some of the quantities have been normalised. *** The thickness distribution of the blade along its length is determined by the chord length and the designation of NACA profile applied at each section.*

Radius (m)	*Chord (m)*	*Twist (°)*	*Profiles ****	*Thickness (%)*
0.00	0.600	0.00	Circular	100
0.50	0.600	0.00	Circular	100
1.00	1.366	12.4	NACA 63-240	40
2.00	1.294	13.2	NACA 63-235	35
3.00	1.223	11.4	NACA 63-230	30
4.00	1.151	9.68	NACA 63-230	30
5.00	1.079	8.05	NACA 63-225	25
6.00	1.008	6.53	NACA 63-225	25
7.00	0.936	5.13	NACA 63-222	22
8.00	0.864	3.87	NACA 63-220	20
9.00	0.793	2.77	NACA 63-220	20
10.00	0.721	1.85	NACA 63-218	18
11.00	0.649	1.12	NACA 63-216	16
12.00	0.574	0.59	NACA 63-216	16
13.00	0.505	0.32	NACA 63-215	15
13.15	0.494	0.29	NACA 63-214	14

Table 4. Radial distribution of the out of plane loads on the wind turbine blade applied in the optimisation study [26].

Radius (m)	*Load (N/m)*
1	3710
2	3510
3	3320
4	3120
5	2930
6	2730
7	2540
8	2340
9	2150
10	1960
11	1760
12	1570
13	1370

Table 5. Outline of the design variables and their limits.

Variable	*Description*	*Lower Limit*	*Upper Limit*
x_1	Triaxial plies $S_0 - S_{10}$	3	5

x_2	Triaxial plies $S_0 - S_9$	0	5
x_3	Triaxial plies $S_0 - S_8$	0	5
x_4	Triaxial plies $S_0 - S_7$	0	5
x_5	Triaxial plies $S_0 - S_6$	0	5
x_6	Triaxial plies $S_0 - S_5$	0	5
x_7	Triaxial plies $S_0 - S_4$	0	5
x_8	Triaxial plies $S_0 - S_3$	0	5
x_9	Triaxial plies $S_0 - S_2$	0	5
x_{10}	Triaxial plies $S_0 - S_1$	0	5
x_{11}	UD plies $S_0 - S_{10}$	1	10
x_{12}	UD plies $S_0 - S_9$	0	10
x_{13}	UD plies $S_0 - S_8$	0	10
x_{14}	UD plies $S_0 - S_7$	0	10
x_{15}	UD plies $S_0 - S_6$	0	10
x_{16}	UD plies $S_0 - S_5$	0	10
x_{17}	UD plies $S_0 - S_4$	0	10
x_{18}	UD plies $S_0 - S_3$	0	10
x_{19}	UD plies $S_0 - S_2$	0	10
x_{20}	UD plies $S_0 - S_1$	0	10
x_{21}	Biaxial plies $S_0 - S_{10}$	1	5
x_{22}	Biaxial plies $S_0 - S_9$	0	5
x_{23}	Biaxial plies $S_0 - S_8$	0	5
x_{24}	Biaxial plies $S_0 - S_7$	0	5
x_{25}	Biaxial plies $S_0 - S_6$	0	5
x_{26}	Biaxial plies $S_0 - S_5$	0	5

x_{27}	Biaxial plies $S_0 - S_4$	0	5
x_{28}	Biaxial plies $S_0 - S_3$	0	5
x_{29}	Biaxial plies $S_0 - S_2$	0	5
x_{30}	Biaxial plies $S_0 - S_1$	0	5
x_{31}	Balsa core drop off	0	9
x_{32}	Number of shear webs	1	2

Table 6. Parameters required for Puck failure criterion.

Material Parameter	*Value*
Tensile failure strain, ε_{1T} (%)	2.807
Compressive failure strain, ε_{1C} (%)	-1.754
Mean stress magnification factor, $m_{\sigma f}$	1.3
In-plane shear strength, S_{12} (MPa)	73
In-plane transverse tensile strength, Y_T (MPa)	-145
In-plane transverse compressive strength, Y_C (MPa)	40
Failure envelope shape parameters, $p_{\parallel\perp}^{(+)}, p_{\perp\parallel}^{(+)}$	0.3
Failure envelope shape parameters, $p_{\perp\parallel}^{(-)}, p_{\perp\perp}^{(-)}$	0.25

Table 7. Information on the set-up of the genetic algorithm.

Population Size	*Total Generations*	*Retained Individuals*	*Chance of Mutation*
25	200	5	0.03 - 0.05

Table 8. The optimum values for each of the design variables from the genetic search algorithm.

Variable	*Solution 1*	*Solution 2*	*Solution 3*	*Solution 4*	*Solution 5*
x_1	3	3	3	3	3
x_2	0	0	0	0	0
x_3	0	0	0	0	0

x_4	0	0	0	0	0
x_5	0	0	0	0	0
x_6	0	0	0	0	0
x_7	1	1	1	1	1
x_8	0	0	0	0	0
x_9	0	0	0	0	0
x_{10}	0	0	0	0	0
x_{11}	2	2	2	2	2
x_{12}	6	6	6	6	6
x_{13}	3	3	2	2	3
x_{14}	2	2	3	3	2
x_{15}	1	1	1	1	1
x_{16}	0	0	0	0	0
x_{17}	1	1	1	1	1
x_{18}	0	0	0	0	0
x_{19}	1	1	0	0	1
x_{20}	2	2	2	2	2
x_{21}	1	1	1	1	1
x_{22}	1	1	1	1	1
x_{23}	0	0	0	0	0
x_{24}	0	0	0	0	0
x_{25}	0	0	0	0	0
x_{26}	0	0	0	0	0
x_{27}	0	0	1	1	1
x_{28}	0	0	0	0	0
x_{29}	0	0	0	0	0
x_{30}	0	0	0	0	0

x_{31}	1	7	0	1	0
x_{32}	1	1	1	1	1

Table 9. Details of the composite layups for Solution 1 optimum blade for the three main sections of the blade: the spar caps, outer aerodynamic shells and the shear webs.

	Spar Caps			***Outer Shells***		***Web***		
0.00	UD x 18	TRIAX x 4	Gelcoat	TRIAX x 4	Gelcoat	BIAX	Core	BIAX
1.00	UD x 18	TRIAX x 4	Gelcoat	TRIAX x 4	Gelcoat	BIAX	Core	BIAX
2.00	UD x 18	TRIAX x 4	Gelcoat	TRIAX x 4	Gelcoat	BIAX	Core	BIAX
3.00	UD x 18	TRIAX x 4	Gelcoat	TRIAX x 4	Gelcoat	BIAX	Core	BIAX
4.00	UD x 16	TRIAX x 4	Gelcoat	TRIAX x 4	Gelcoat	BIAX	Core	BIAX
5.00	UD x 15	TRIAX x 4	Gelcoat	TRIAX x 4	Gelcoat	BIAX x 2		
6.00	UD x 15	TRIAX x 4	Gelcoat	TRIAX x 4	Gelcoat	BIAX x 2		
7.00	UD x 14	TRIAX x 3	Gelcoat	TRIAX x 3	Gelcoat	BIAX x 2		
8.00	UD x 14	TRIAX x 3	Gelcoat	TRIAX x 3	Gelcoat	BIAX x 2		
9.00	UD x 13	TRIAX x 3	Gelcoat	TRIAX x 3	Gelcoat	BIAX x 2		
10.00	UD x 11	TRIAX x 3	Gelcoat	TRIAX x 3	Gelcoat	BIAX x 2		
11.00	UD x 8	TRIAX x 3	Gelcoat	TRIAX x 3	Gelcoat	BIAX x 2		
12.00	UD x 2	TRIAX x 3	Gelcoat	TRIAX x 3	Gelcoat	BIAX		
12.50	UD x 2	TRIAX x 3	Gelcoat	TRIAX x 3	Gelcoat	BIAX		
13.00	UD x 2	TRIAX x 3	Gelcoat	TRIAX x 3	Gelcoat	BIAX		
13.15	UD x 2	TRIAX x 3	Gelcoat	TRIAX x 3	Gelcoat	BIAX		

Table 10. Breakdown of the results of the optimum designs found by the genetic algorithm.

	Solution 1	*Solution 2*	*Solution 3*	*Solution 4*	*Solution 5*	*Reference Blade*
Fitness (kg)	387.2	387.9	388.3	388.4	389.3	497.0
Mass (kg)	383.1	383.7	377.0	377.2	386.0	497.0
Mass Saving (%)	22.9	22.8	24.1	24.1	22.3	-
Cost Savings (%)	15.5	15.4	16.3	16.3	15.1	-
δ_{tip} *(mm)*	809	809	824	823	807	800
Tip Rotation (°)	10.6	10.6	10.7	10.7	10.6	7.9
Max $f_E(FF)^+$	0.081	0.081	0.081	0.081	0.081	0.197
Max $f_E(FF)^-$	0.148	0.147	0.147	0.147	0.148	0.254
Max $f_E(IFF)^A$	0.730	0.731	0.742	0.743	0.720	0.745

Max $f_E(IFF)^B$	0.238	0.238	0.238	0.238	0.238	0.136
Max $f_E(IFF)^C$	0.234	0.234	0.234	0.234	0.234	0.200
Radial Location of Centre of Mass (m)	4.38	4.38	4.41	4.41	4.37	4.25
Generation Determined	190	195	192	175	176	-